

# Effect of Shield-Can on Dynamic Response of Board-Level Assembly

Da Yu

Jae Kwak

Seungbae Park<sup>1</sup>

Mechanical Engineering Department,  
State University of New York at Binghamton,  
Binghamton, NY 13905

Soonwan Chung

Ji-Young Yoon

Mechatronics and Manufacturing  
Technology Center,  
Samsung Electronics Co., LTD.,  
Suwon, 443-803, South Korea

*In order to protect the electronic components of electronic devices on a printed circuit board (PCB) against electromagnetic radiation, a conductive shield-can or box is normally attached to the PCB covering the electronic components. In particular, handheld electronic devices are prone to be subjected to drop impact. This means that the products would experience a significant amount of out-of-plane deformation along the PCB, which may cause stresses eventually resulting in solder joint failures. The attached shield-can could provide additional mechanical strength and minimize the out-of-plane deformation, especially where the electronic package is located. In this study, both the dynamic responses of the PCB and the characteristic life of solder joints with different shield-can designs were investigated, which are seldom explored by other researchers. In the board-level drop tests, a noncontact full-field optical measurement technique, digital image correlation (DIC) with images taken by stereo-high-speed cameras, was used to obtain full-field displacement data showing the dynamic responses of the PCB during the drop impact. PCBs with a fine ball grid array (FBGA) package were prepared with various types of shield-can attached. From the experimental results the effects of different shield-can types, varying in shape and size on the dynamic responses of the PCB, were analyzed. In addition, the number of drops to failure for each shield-can was also recorded by an event detector. Using ANSYS/LS-DYNA, an accurately validated finite element model has been developed. Then the stress analysis could be performed in order to study the failure mechanism by finding the maximum tensile stress of the solder joints during the drop impact and correlate the stress results with the characteristic life of solder joint. [DOI: 10.1115/1.4007118]*

## 1 Introduction

The most common solution for controlling electromagnetic compatibility might be shielding by using metal enclosures so that it keeps harmful interference out or unwanted emissions in. Especially at the PCB level, a small shield-can can be selectively applied to the problem areas of a circuit, directly protecting the components from electromagnetic emission. In addition, since handheld devices are widely used in our daily life, the drop impact is prone to occur to those devices, which not only causes the mechanical failure of their housings, but also induces the failure of components mounted on the PCB. The primary cause of these failures is excessive flexing of the circuit board due to input acceleration to the board created by dropping the handheld electronic product, which causes relative motion between the PCB and the attached components, resulting in component, interconnect, or board failures [1]. From a mechanical engineering standpoint, a shield-can could provide more mechanical strength to the PCB, which may reduce board deflection when it is subjected to a drop event.

A great amount of analytical and experimental research has been reported regarding the board-level drop test over the past few years [2–7] to investigate the failure mechanism and predict the impact life. However, most of this research was achieved without consideration of the attached shield-can effect. This study is to investigate the effect of the shield-can and its design on the dynamic responses of the PCB and impact life.

For the experiments in this work, the PCB with an FBGA package solder jointed was prepared with various designs of shield-cans attached. These test vehicles were mounted on the drop table. A board-level drop test was conducted. Additionally, by using stereo high-speed cameras, images were collected at a rate of 14,000 frames per second before and after the shock table strikes the rigid surface. Then, the DIC was applied by importing these images to monitor and document the dynamic responses of the PCB during drop impact. This experimental technique was well validated by previous works in terms of the accuracy of deformation and strain calculation in DIC [8–12]. Therefore, the effect of the initial gap and shield-can design, including the mounting type on the dynamic responses of the PCB, was experimentally analyzed.

In contrast to the drop test, which is time-consuming and laborious, a transient analysis using finite element analysis (FEA) can easily generate a full-field out-of-plane deformation distribution of a PCB during the drop impact. Therefore, a 3D FEA model has been developed to analyze the dynamic responses of PCBs using ANSYS/LS-DYNA<sup>TM</sup>. For validating the FEA model, a special technique was developed by introducing a fictitious bonding material between the shield-can and the mounting surface to represent their dynamic interactions during the impact duration. Finally, the stress analysis on the solder joints was achieved to investigate the failure mechanism and identify the failure criteria in the drop test.

Both the simulation studies and experimental results are useful since they provide an insight into the drop event and improve the design of the shield-can in order to increase the drop reliability under impact loading.

## 2 Experiment Setup

A typical board-level drop test setup [9,10] is shown in Fig. 1. The PCB was mounted to the drop table of a Lansmont<sup>®</sup> M23 drop tester with the component and shield-can facing down. The

<sup>1</sup>Corresponding author.

Contributed by the Electronic and Photonic Packaging Division of ASME for publication in the JOURNAL OF ELECTRONIC PACKAGING. Manuscript received October 25, 2011; final manuscript received June 20, 2012; published online July 23, 2012. Assoc. Editor: Sandeep Tonapi.

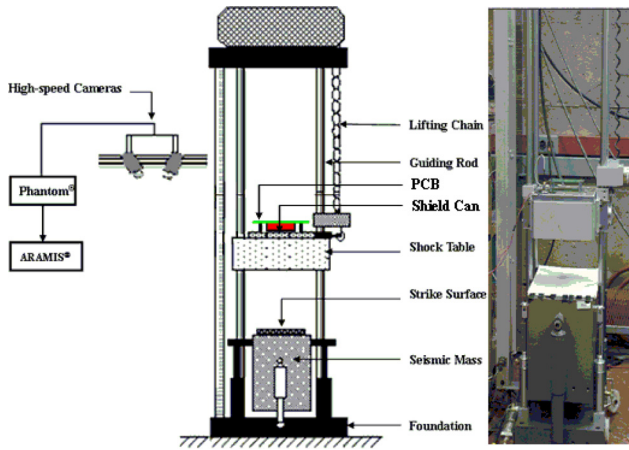


**Fig. 1 Experimental setup: drop test facility and the DIC measurement system**

shock table was raised to the specified height and dropped on the strike surface while measuring the g-level, pulse duration, and pulse shape. Multiple drops may be required while adjusting the drop height and strike surface to achieve the specified g-levels and pulse duration. The test board and test setup did not strictly follow the JEDEC test standard in this work, however, in order to provide a reproducible assessment of the drop test performance of the shield-can, the JEDEC standard half-sine, the pulse with 1500 g peak acceleration and 0.5 ms pulse time (see Fig. 2), was obtained and used as the input pulse.

### 2.1 Digital Image Correlation With High-Speed Cameras.

The key requirement of this experiment is to accurately measure the time-history response of the PCB assembly to the impact load. Therefore, the high-speed imaging system was integrated with the DIC system to analyze the full-field image series captured by the cameras.

Digital image correlation is a full-field optical measurement technique in which both the in-plane and out-of-plane deformations can be computed by comparing the pictures of the target object at the initial and deformed stages. Thousands of unique correlation areas (known as facets) are defined across the entire imaging area. As shown in Fig. 3, a random speckle pattern with high contrast is applied over the PCB surface using black and white paint sprays. Then these facet centers are tracked, in each successive pair of images, with an accuracy of up to one hundredth of a pixel. Finally, by using the principles of

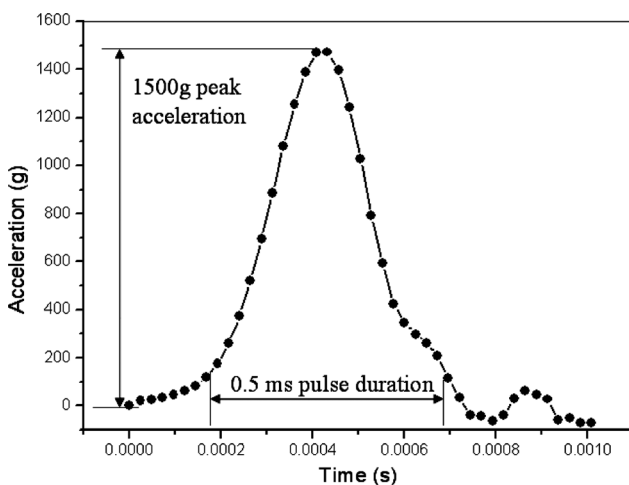


**Fig. 2 Half-sine input pulse for the shock table**

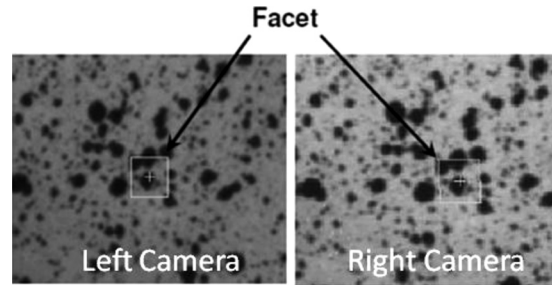


**Fig. 3 Images from stereo-cameras showing the correlation facet**

photogrammetry, the coordinates of each facet are determined for each set of images. The results are the 3D shape of the component, the displacements, and the strains. Rigid-body motion can first be quantified and then removed to reveal relative deformations [9–11].

A stereo high-speed digital camera has been set up to capture pictures of the board surface during impact frame by frame, with a frequency of up to 14,000 frames per second. Pre- and post-impact portions of the drop were extracted in the form of series of images from Phantom<sup>®</sup>. These images were then exported to ARAMIS<sup>®</sup> for solving the full-field deformations, 3D shape, and the strain of the PCB. The corners of the PCB were chosen, depending on how the PCB was mounted to the drop table, as reference points for the purpose of ‘movement correction’ in ARAMIS to eliminate rigid-body motion so that the relative out-of-plane deformation was calculated.

A preliminary experiment was conducted to correlate results from the DIC with accelerometer measurements taken simultaneously during the drop impact. A good correlation was obtained between both measurements of output acceleration. This provided sufficient confidence in the current testing methodology and the DIC system [12].

### 2.2 Test Vehicle.

The test board (100 mm × 50 mm × 0.8 mm) has four mounting screw holes and was mounted to the drop table through standoffs (washers). A 332FBGA package,

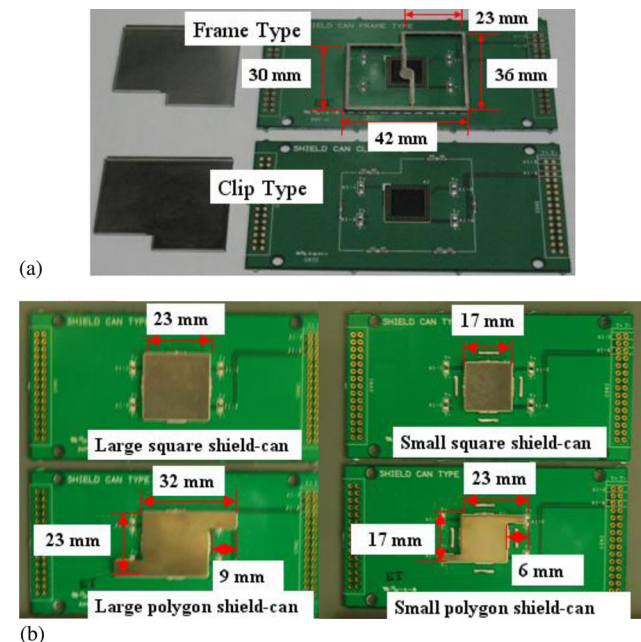


**Fig. 4 (a) Test vehicles with two different connecting methods: (b) test vehicles with different shield-can sizes and shapes**

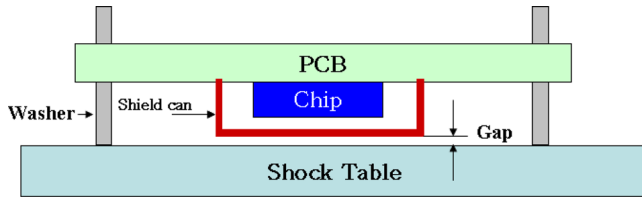
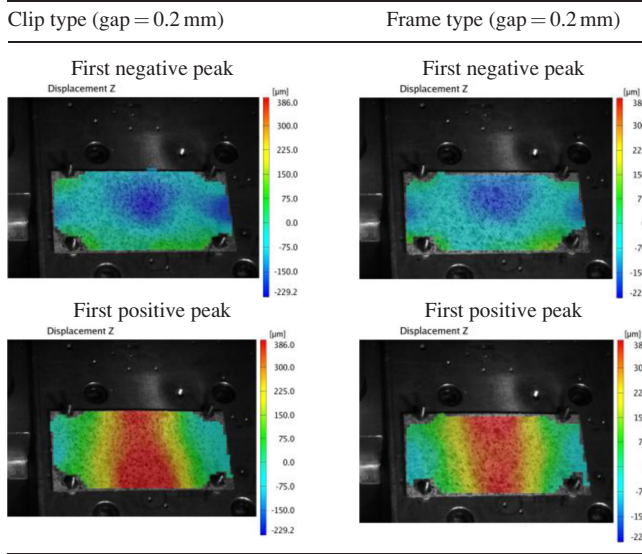


Fig. 5 Sketch of the washer and shield-can

Table 1 Out-of-plane deformation contour plots for clip type and frame type shield-cans



14 mm × 14 mm, mounted with 0.3 mm diameter lead-free solder balls (SAC405) in 0.5 mm pitch is assembled on the PCB.

The shield-can, which is made of a thin aluminum sheet (0.2 mm in thickness), of the same design, is attached to the PCB through a frame type or clip type connection. Figure 4(a) shows a frame welded on the PCB. The frame is slightly larger than the edge circumference of the shield-can walls in order to hold the shield-can by the spring force of the flexing walls. On the contrary, for the clip type connection, as the lower PCB shows in Fig. 4(a), several U-clips are welded onto the PCB to clamp the shield-can edges.

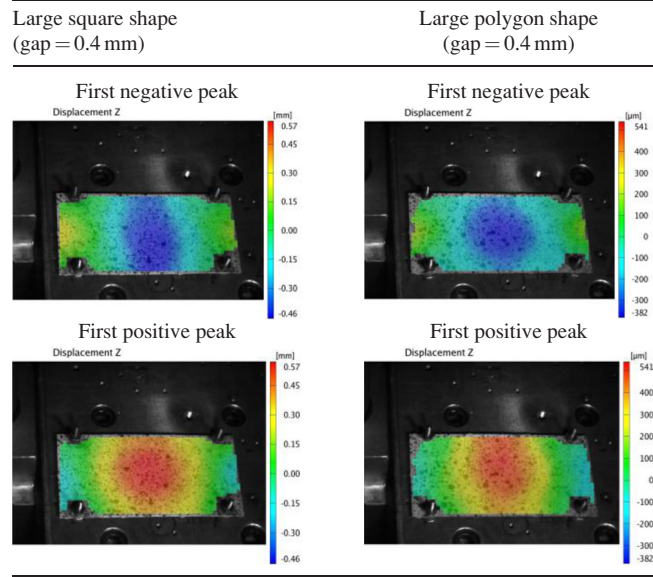
As shown in Fig. 4(b), the clip type connection is applied to all shield-cans of different designs with different sizes in the following impact tests to investigate the effects of the shield-can size and shape. The weight of the small square, large square, small polygon, and large polygon shield-cans are 0.55 g, 0.97 g, 0.65 g, and 1.21 g, respectively.

### 3 Board-Level Drop Test Results

The height of the washer is slightly higher than the height of the shield-can to apply different initial gap sizes between the bottom surface of the shield-can and the shock table (see Fig. 5). During the drop impact, the flexural oscillation of the PCB was restrained by the small initial gap, which mimics the dynamic behavior of a PCB normally observed in ultracompact handheld electronic devices.

**3.1 Effects of Shield-Can Connection Type.** The shield-can connection can be categorized into frame type and clip type connections. Therefore, the effects of the shield-can connection type on the dynamic responses of the PCB were investigated through drop tests with a 0.2 mm initial gap.

Table 2 Out-of-plane deformation contour plots for large polygon and square shaped shield-cans



The DIC provides a contour plot of the displacements and strains along with the time-history data. The full-field deformation contour plot of the PCB (as shown in Tables 1 and 2) reveals the quantized location of maximum displacement, where the electronic component is most likely to fail on the PCB.

The time-history data of the maximum deformation points, which are around the PCB's center (see Table 1), were also extracted from the DIC. According to Fig. 6, there is more rigid mechanical support to the PCB for the frame type than the clip type connection, as indicated by a slight reduction of the out-of-plane deformation. Since the shield-can configurations are the same for both connection methods, the bending characteristic is similar in terms of the vibration frequency, while the amplitude is different, as shown in Fig. 6. It can be concluded that the clip type connection provides almost the same mechanical support as the frame type. We could expect a similar impact life of an electronic package for those two connection types. However, compared to the frame type connection, the clip type connection has unique advantages in terms of the efficient use of the PCB space, cost reduction, and easy repairs. Therefore, the clip type

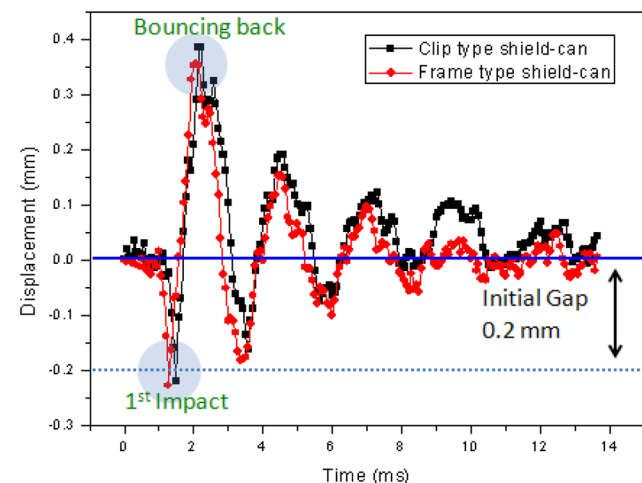
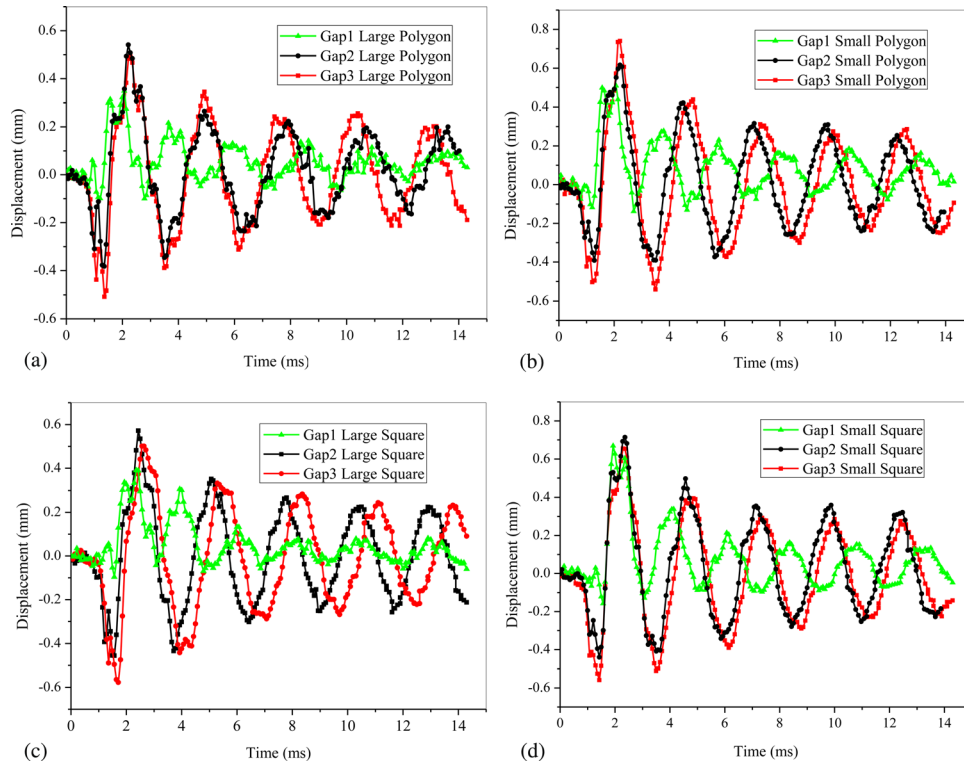


Fig. 6 Out-of-plane displacement of the maximum deformation point for different connection type shield-cans



**Fig. 7** (a) Out-of-plane displacement of the maximum deformation point for a large polygon shaped shield-can, (b) out-of-plane displacement of the maximum deformation point for a small polygon shaped shield-can, (c) out-of-plane displacement of the maximum deformation point for a large square shaped shield-can, and (d) out-of-plane displacement of the maximum deformation point for a small square shaped shield-can

connection is more recommended in the handheld electronic devices.

**3.2 Effects of Initial Gap.** In the following drop tests, the initial gaps chosen are: Gap 1: 0.1 mm, Gap 2: 0.4 mm, and Gap 3: 0.5 mm. Since the PCB's bending mode shape depends on the shield-can configurations, for a square shaped shield-can, the PCB has the maximum out-of-plane deformation around its center, as shown in Table 2, which is slightly different from the polygon shaped shield-can.

The bending down process of the PCB is limited by the initial gap size. As indicated in Fig. 7, the negative peak amplitude increases as the initial gap increases. According to the comparison between Figs. 7(a) and 7(c), more rigid mechanical support to the PCB for the polygon shaped shield-can than the square shape is indicated by a reduction of the maximum deformation (from  $-0.57$  mm to  $-0.51$  mm for both large shield-cans).

**3.3 Effects of Shield-Can Shape and Size.** As is clearly indicated in Fig. 8, the time-history displacement data of the PCB's center point shows that the first negative peaks are almost the same for both cases. However, the amplitude of the following positive peaks decreases as the shield-can size increases, simply because the large shield-can will apply more constraint to the PCB during its bouncing-back process. The oscillation frequency of the large shield-can is lower than the small one, also indicating that the small shield-can provided less constraint. In addition, the decay rate of the large shape shield-can amplitude was faster due to more energy being dissipated through the large shield-can.

#### 4 Characteristic Life

In order to investigate the effect of the shield-can size and shape on the reliability of the electronic component, an event detector was applied to constantly monitor the resistance of the

daisy chained circuits (see the bottom edge loop and bottom loop in Fig. 9) throughout the test and record the number of drops to failure. A failure was recorded when the resistance of the daisy chain exceeded the  $1000 \Omega$  threshold resistance for 200 ns at least four times in a sequence of six drops. Square and polygon shaped shield-cans were tested at Gap 2 (0.4 mm) with five test samples at each size.

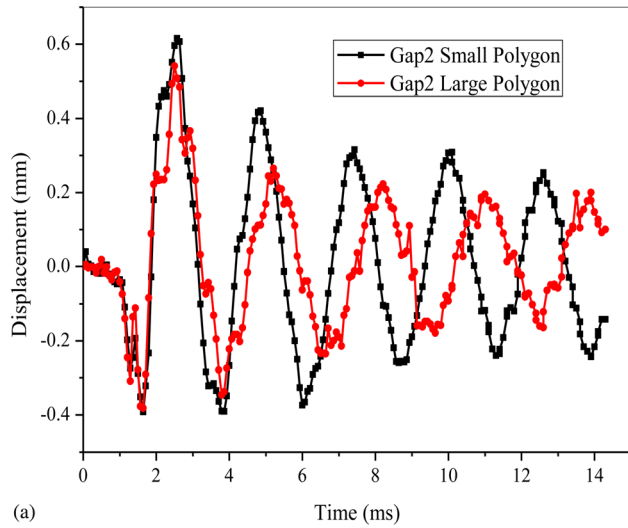
A failure analysis of the drops to failure from the impact tests was conducted using a two-parameter Weibull distribution model

$$F(t) = 1 - \exp \left[ - \left( \frac{t}{\eta} \right)^\beta \right] \quad (1)$$

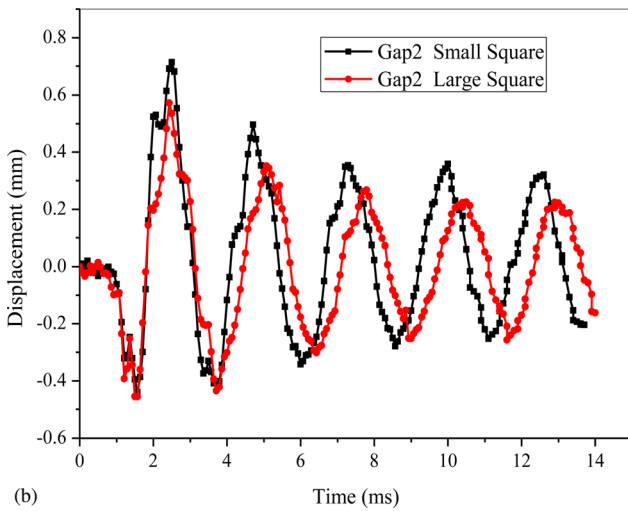
where  $F(t)$  is the cumulative failure distribution function,  $\eta$  is referred to as the characteristic life and is the number of failure cycles at which 63.2% of the devices failed, and  $\beta$  is the shape parameter.

The drop reliability is shown as a Weibull distribution in Fig. 10. In this test, the characteristic life ( $N_{63}$ ) of the large square shield-can, small square shield-can, and small polygon shield-can are 166, 434, and 547 drops, respectively. It is clearly shown that the small square shield-can increases the reliability of the package to the drop impact. According to experimental results, the outer daisy chained circuit (monitored by channel 4 and marked as a blue line in Fig. 9) fails much earlier than the inner daisy chained circuit (monitored by channel 2 and marked as a red line in Fig. 9)

Conventionally, the out-of-plane deformation of the attached PCB is always of major interest to manufacturers since it relates to the stress causing failure for the solder balls [13,14]. However, contrary to this common perception, the small square shield-can, with a higher PCB deflection, has shown a longer impact life of the package, indicating lower stress in the solder balls. Therefore, a stress analysis of the solder joints is numerically performed to investigate the failure mechanism in relation to the PCB deflections.



(a)



(b)

**Fig. 8** (a) Out-of-plane displacement comparison of the maximum deformation point for a polygon shaped shield-can; (b) out-of-plane displacement comparison of the maximum deformation point for a square shaped shield-can

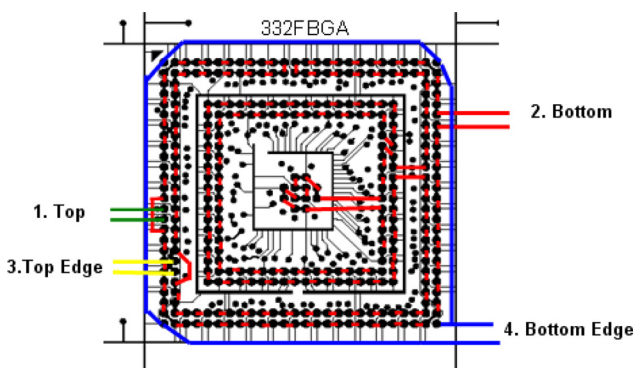


**Fig. 9** Daisy chained circuits for the 332FBGA

## 5 Finite Element Model

A 3D finite element (FE) model was built and the input-G method was used to effectively perform a transient analysis by using ANSYS/LS-DYNA. The PCB and shield-can were modeled with shell163 while the screws, washers, and package were modeled in detail with solid164. Solder balls at the corner were

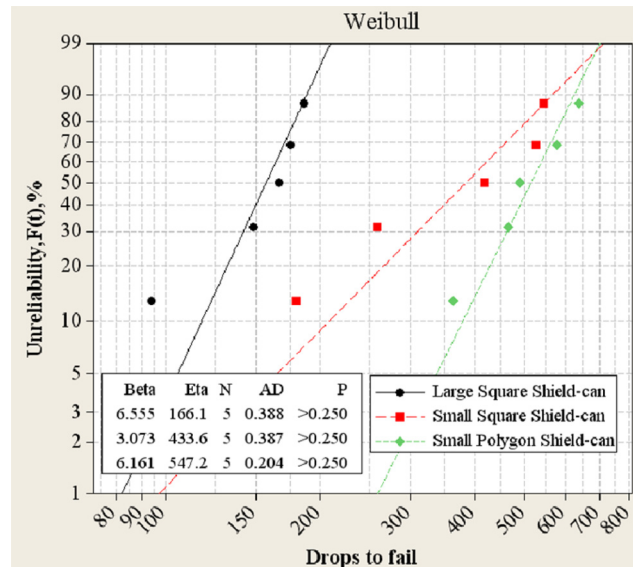


**Fig. 10** Weibull distribution of drop failures for different shield-cans

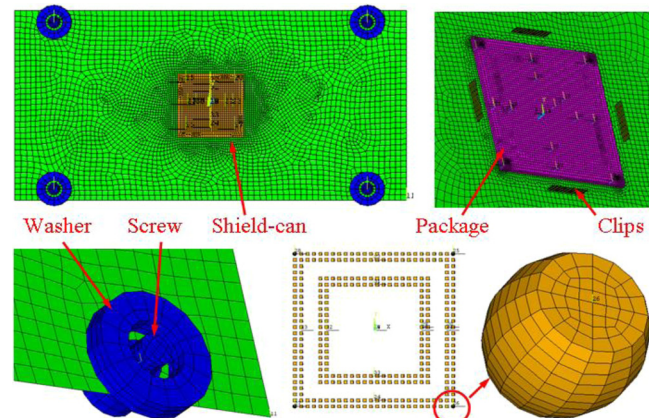


**Fig. 11** Finite element model of the PCB assembly

modeled in detail while equivalent cubes were used to represent all other solder balls in this work (see Fig. 11).

All components were treated as isotropic material, except for the solder joint, as shown in Table 3. The trilinear elastic-plastic model was applied to the SAC405 solder joints as the stress-strain relationship schematically shown in Fig. 12 [14]. The Young's modulus of the PCB, which is a critical parameter in the characterization of the dynamic behavior, was obtained from a tensile test.

Nodes on the bottom surface of the washers and screws along with the thread of the screws were constrained in all degrees of freedom (Fig. 13), which was representing the experimental conditions. Several contact pairs had to be defined in the simulation model to treat the contact during the impact event. Thus, surface to surface contact was defined for the interfaces of the PCB/washer and the PCB/screw. Auto surface to surface contact was used to define the contact between the shield-can bottom and top surfaces of the shock table, which was modeled as a rigid surface.

Both the clips and the shield-can were modeled by a shell element. A fictitious bonding material was created as a medium to connect the shield-can with the clips, as shown in Fig. 14. In reality, the shield-can is clamped by the clips through the friction under the spring (flexure) force between them. During the bending deformation of the PCB, the shield-can may slide along the frame

**Table 3 Material properties**

Materials	Young's modulus (GPa)	Poisson's ratio	Density (kg/m <sup>3</sup> )
PCB	32	0.28	2750
Substrate	22	0.28	2000
Mold compound	20	0.30	1890
Die	131	0.30	2330
Frame and can	223	0.28	7930
Standoff and screw	200	0.3	7870
Shock table	210	0.29	7800

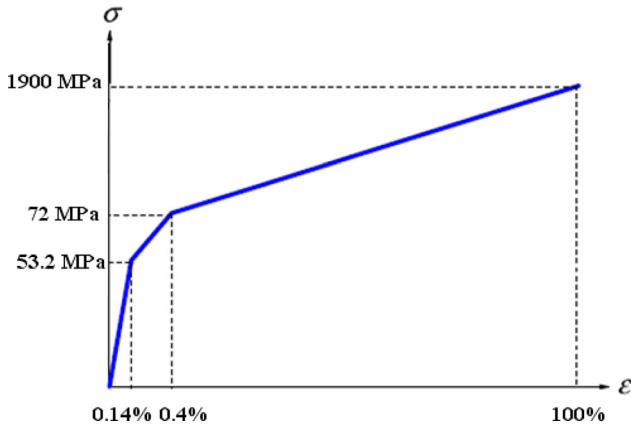


**Fig. 12 Elastic-plastic-model for the SAC405 [14]**

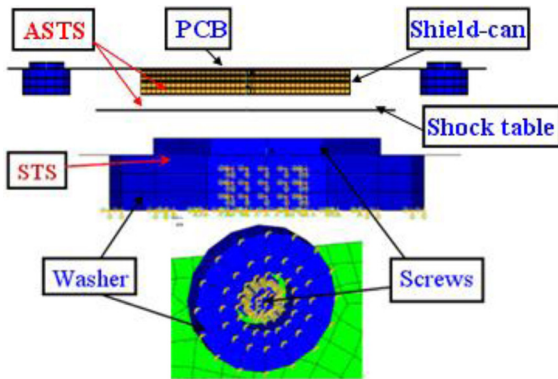


**Fig. 13 Define the boundary conditions and contact pairs**

sidewall. Therefore, a fictitious bonding material, as an interface, can deform and can be made to approximately match the relative displacement by varying its flexibility. In this model, the fictitious bonding material was chosen to be very soft with Young's modulus equal to 1 GPa. The correlation between the simulation and experimental results was dramatically improved through this method [15,16].

**5.1 Simulation Results.** Figure 15 shows a reasonably good agreement between the simulation and experimental results (Gap 2) due to the fact that the vibration frequency and phase for both the simulation and experiment closely match one another. However, according to the time-history displacement response results, the simulation overestimated the rebound amplitudes, indicating that there were additional constraints or energy dissipation unaccounted for in the simulation.

Through the comparison of the experimental results, the errors of the first displacement peak between the simulation and experiment are 27% (large square shield-can) and 28% (small square

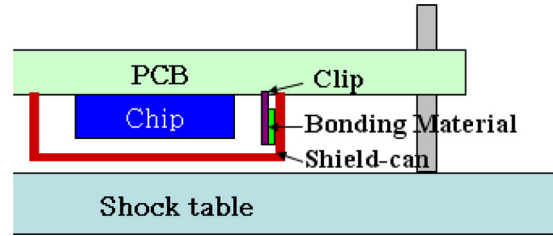
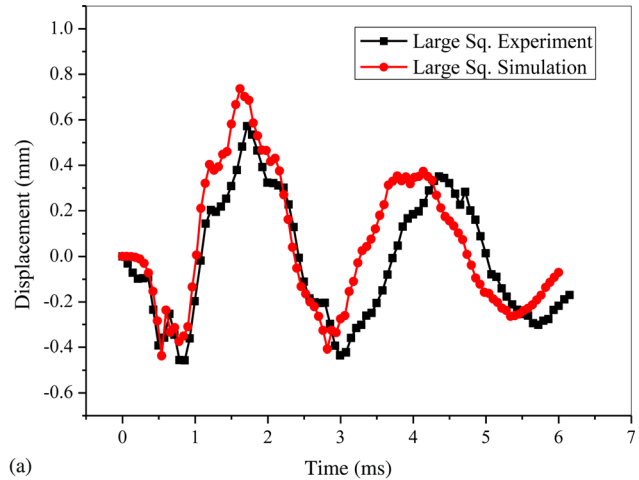
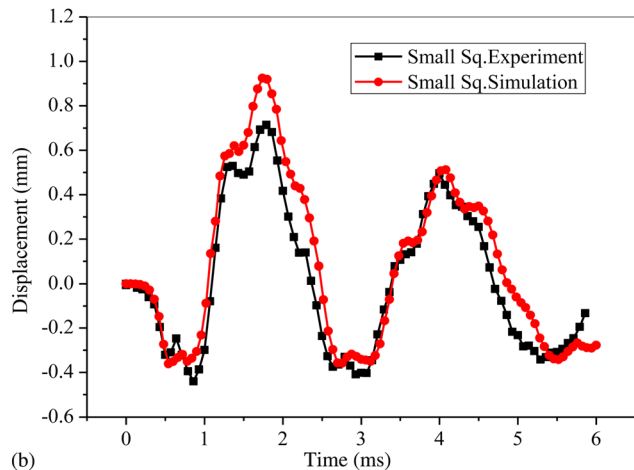


**Fig. 14 Define the fictitious bonding material**



(a)



(b)

**Fig. 15 (a) Simulation results for a large square shaped shield-can; (b) simulation results for a small square shaped shield-can**

shield-can). This validated FE model is a prerequisite for the further stress analysis of the critical solder joints.

**5.2 Stress Analysis.** The solder joints in the FEA model were observed to have the stress concentration along the solder/PCB interface at the outermost corner (see Fig. 16), which correlates well with the typical failure mode. The failed test vehicles were cross-sectioned and were more frequently found to have a crack along the solder/PCB interface rather than on the component side of the outermost corner (see Fig. 17).

The peeling stress ( $S_z$ ) of the critical solder joint is used as the failure criteria during the drop impact in this work, which is one order of magnitude larger than the other normal stresses and shear stresses in the FEA model. This is also validated by other modeling works considering a drop event [17,18].

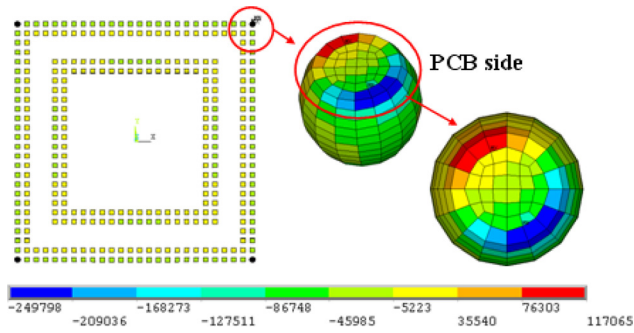


Fig. 16 Peeling stress distributions of the solder joints

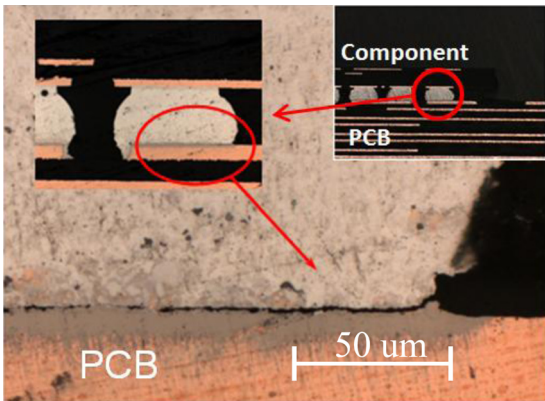


Fig. 17 Cross-section of the typical failed solder joint

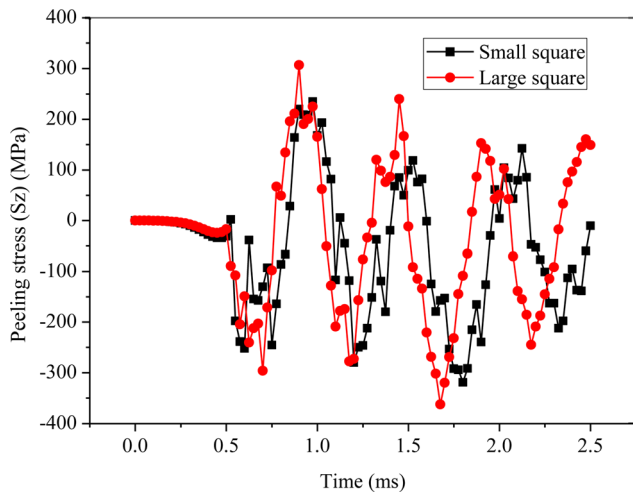


Fig. 18 The maximum peeling stress of critical solder joints in the FEA model

The maximum peeling stresses obtained from the PCB side of critical solder joints in the large and small square shield-can FEA models are compared in Fig. 18. It is interesting to note that the small square shield-can shows lower tensile stress (positive peaks)

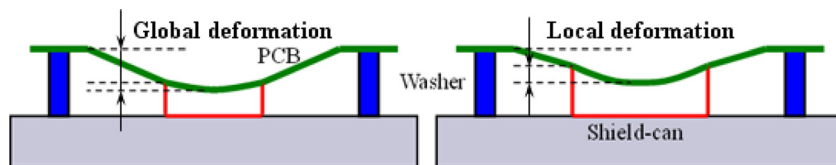
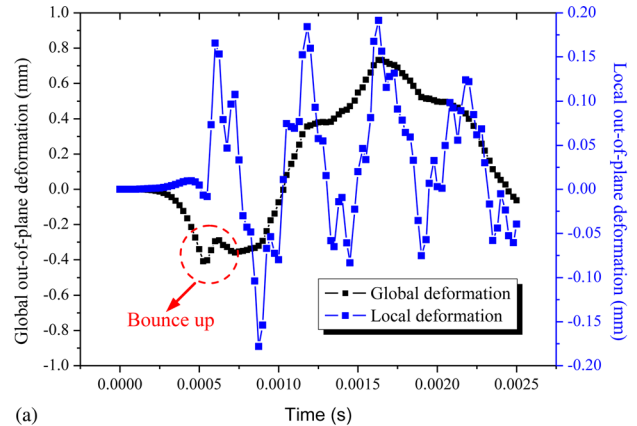
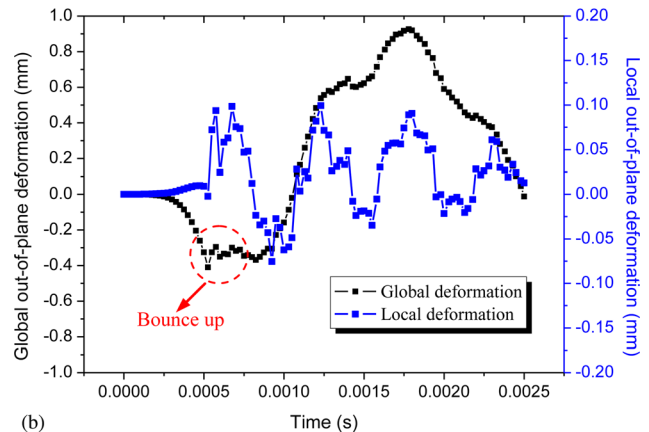


Fig. 19 Sketch of local and global out-of-plane deformation of the PCB



(a)



(b)

Fig. 20 (a) Global and local out-of-plane deformation of a large square shield-can; (b) global and local out-of-plane deformation of a small square shield-can

despite the higher global out-of-plane deformation. More detailed reasons will be discussed in the following section. Since the over-stress of solder joints is believed to be the major driver of package failure during the drop impact, the higher tensile stress is more prone to initialize the crack of solder joints, which explains why the small square shield-can (with a maximum  $S_z$  of 234 MPa) has a longer characteristic life than the large one (with a maximum  $S_z$  of 306 MPa).

As illustrated in Fig. 19, the local deformation is defined as the relative out-of-plane deformation of the PCB within the shield-can area while the global deformation represents the overall behavior of the entire PCB. When the shock table hits the strike surface (Fig. 1), the PCB bends downward due to the inertia load and then the shield-can collides onto the shock table. During the impact, a large amount of impact force transmitted through the shield-can to the local PCB within the shield-can makes the local PCB instantly bend up, which explains why a bounce up is shown (see Fig. 20) in the global deformation curve. Thereafter, the flexural oscillation of the local PCB was excited at a much higher frequency, as shown in the time-history data of the local out-of-plane deformation (see Fig. 20).

**Table 4 Impact life prediction results**

Shield-can types	Maximum peeling stress (MPa)	Impact life (drops)	Predicted impact life (drops)	Difference (%)
Small square	234	434	416	-4.15
Large square	306	166	172	+3.61
Small polygon	214	547	557	+1.82
Large polygon	295	190	193	+1.58

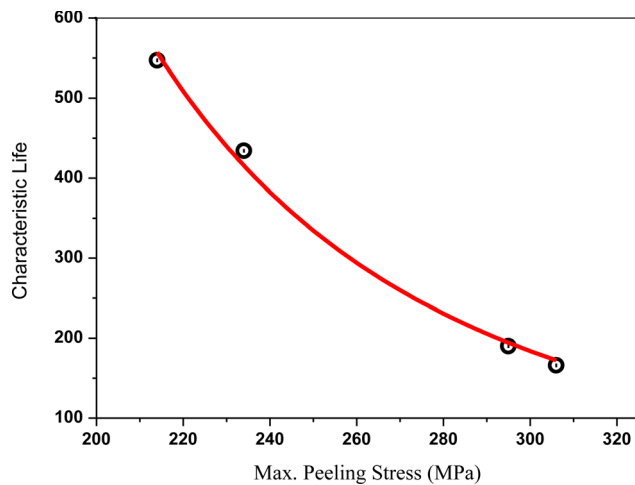


**Fig. 21 Correlation of the impact life and maximum peeling stress**

Since the solder joint interfacial failure is mainly induced by the relative motion between the PCB and the attached components during its bending process after impact, the local flexural oscillation is more crucial to the reliability of the package than the PCB's global behavior. According to Figs. 18 and 20, the local deformation of the small shield-can is smaller than large the shield-can, as well as the maximum peeling stress. Therefore, the small sized shield-can stiffens the localized area around the package, lowering its out-of-plane deformation, and increases the impact life of the package.

**5.3 Drop Impact Life Prediction Model.** The FE model is well validated in terms of the dynamic responses of the PCB during the board-level drop impact. The impact life prediction model is then proposed to evaluate the drop impact reliability.

The maximum peeling stress of the critical solder obtained from the FEA models are listed in Table 4. A power law was applied to correlate the maximum peeling stress of the critical solder with the impact life [3]

$$N_{63} = C_1 \sigma_2^{C_2} \quad (2)$$

where  $N_{63}$  is the characteristic life,  $\sigma_2$  is the maximum peeling stress (MPa) in the critical solder joint,  $C_1$  and  $C_2$  are the correlation constants,  $2.4318 \times 10^{10}$  and  $-3.2784$ , respectively (see Fig. 21). It should be noted that the correlation constants used in the drop impact life prediction model are model and tester dependent. However, the relative comparison of the impact performance based on the impact life prediction model should still be valid [3]. It shows good correlation between the predicted impact life and the drop test results since the uncertainty in the impact life predictions is within  $\pm 5\%$  (see Table 4).

## 6 Conclusions

The dynamic responses of a PCB under the board-level drop test were investigated with the aid of a noncontact full-field optical measurement technique, the digital image correlation.

The effects of the shield-can design and size were experimentally analyzed. The shield-can, which acts as a mechanical support to the PCB, limits the PCB deflection to reduce its deformation during and after the drop impact. Moreover, the small polygon shaped shield-can is found to be more effective in lowering the flexural oscillation of the local PCB and increases the impact reliability of the package.

A 3D FEA model has been constructed to analyze the dynamic responses of the PCB using ANSYS/LS-DYNA. The validated FE model shows that the small sized shield-can stiffens the localized area around the package by lowering the local deformation, which is directly related to the maximum peeling stress.

## Acknowledgment

The authors appreciate the materials and financial support from Samsung Electronics.

## References

- [1] JEDEC Standard JESD22-B111, 2003, "Board Level Drop Test Method of Components for Handheld Electronic Products."
- [2] Luan, J. E., and Tee, T. Y., 2004, "Novel Board Level Drop Test Simulation Using Implicit Transient Analysis With Input-G Method," Proceedings of the 6th EPTC, Singapore, Dec. 8-10, pp. 671-677.
- [3] Tee, T. Y., Ng, H. S., Lim, C. T., Pek, E., and Zhong, Z., 2004, "Impact Life Prediction Modeling of TFBGA Packages Under Board Level Drop Test," *Microelectron. Reliab.*, **44**, pp. 1131-1142.
- [4] Chai, T. C., Quek, S., Hnin, W. Y., and Wong, E. H., 2005, "Board Level Drop Test Reliability of IC Packages," Proceedings of the 55th ECTC, Lake Buena Vista, FL, May 31-June 3, pp. 630-636.
- [5] Wong, E. H., and Mai, Y.-W., 2006, "New Insights Into Board Level Drop Impact," *Microelectron. Reliab.*, **46** (5-6), pp. 930-938.
- [6] Qu, X., Chen, Z., Qi, B., Lee, T., and Wang, J., 2007, "Board Level Drop Test and Simulation of Leaded and Lead-Free BGA-PCB Assembly," *Microelectron. Reliab.*, **47**(12), pp. 2197-2204.
- [7] Ong, Y. C., Shim, V. P. W., Chai, T. C., and Lim, C. T., 2003, "Comparison of Mechanical Response of PCBs Subjected to Product-Level and Board-Level Drop Impact Tests," Proceedings of the 5th EPTC, Singapore, Dec. 10-12, pp. 223-227.
- [8] Park, S. B., Al-Yafawi, A., Yu, D., Kwak, J., Lee, J., and Goo, N. S., 2008, "Influence of Fastening Methods on the Dynamic Response and Reliability Assessment of PCBs in Cellular Phones Under Free Drop," Proceedings of ITherm 2008, Orlando, FL, May 28-31, pp. 876-882.
- [9] Park, S. B., Shah, C., Kwak, J. B., Jang, C., Chung, S., and Pitarresi, J. M., 2008, "Measurement of Transient Dynamic Response of Circuit Boards of a Handheld Device During Drop Using 3D Digital Image Correlation," *ASME J. Electron. Packag.*, **130**(4), p. 044502.
- [10] Park, S. B., Shah, C., Kwak, J., Jang, C., Pitarresi, J., Park, T., and Jang, S., 2007, "Transient Dynamic Simulation and Full-Field Test Validation for a Slim-PCB of Mobile Phone Under Drop/Impact," Proceedings of the 57th ECTC, Reno, NV, May 29-June 1, pp. 914-923.
- [11] Park, S. B., Yu, D., Al-Yafawi, A., Kwak, J., and Lee, J., 2009, "Effect of Damping and Air Cushion on Dynamic Responses of PCB Under Product Level Free Drop Impact," Proceedings of the 59th ECTC, San Diego, CA, May 26-29, pp. 1256-1262.
- [12] Yu, D., Kwak, J. B., and Park, S., 2010, "Dynamic Responses of PCB Under Product Level Free Drop Impact," *Microelectron. Reliab.*, **50**(7), pp. 1028-1038.
- [13] Kim, J. G. and Park, Y. K., 2004, "Experimental Verification of Drop/Impact Simulation for a Cellular Phone," *Exp. Mech.*, **44**(4), pp. 375-380.
- [14] Wiese, S. and Rzepka, S., 2004, "Time-Independent Elastic-Plastic Behavior of Solder Materials," *Microelectron. Reliab.*, **44**, pp. 1893-1900.
- [15] Yu, D., Kwak, J. B., Park, S., Chung, S., and Yoon, J.-Y., 2009, "Effect of Shield-Can Design on Dynamic Responses of PCB Under Board Level Drop Impact," Proceedings of the ASME IMECE 2009, Lake Buena Vista, FL, Nov. 13-19 pp. 305-310.
- [16] Kwak, J., Yu, D., Park, S. B., Chung, S., Yoon, J.-Y., and Jang, K.-W., 2010, "Effect of Shield-Can for Drop/Shock Behavior of Board Level Assembly," Proceedings of ITherm 2010, Las Vegas, June 2-5, pp. 1-7.
- [17] Tee, T. Y., Ng, H. S., Li, C. T., Pek, E., and Zhong, Z. W., 2003, "Board Level Drop Test and Simulation of TFBGA Packages for Telecommunication Applications," Proceedings of the 53rd ECTC Conference, New Orleans, May 27-30, pp. 121-129.
- [18] Tee, T. Y., Luan, J. E., Pek, E., Lim, C. T., and Zhong, Z. W., 2004, "Advanced Experimental and Simulation Techniques for Analysis of Dynamic Responses During Drop Impact," Proceedings of the 54th ECTC Conference, Las Vegas, June 1-4, pp. 1088-1094.